Charge coupled devices at ESO - Performances and results

Cyril Cavadore and Reinhold J. Dorn and James W. Beletic
European Southern Observatory, Germany

Abstract: The Optical Detector Team at the European Southern Observatory (ESO) is in charge of developing, installing and maintaining all optical detector systems for ESO's La Silla and Paranal observatories. A CCD controller named FIERA was developed in-house 3 years ago to accommodate a variety of new-generation CCDs manufactured by EEV, MIT Lincoln Laboratory and Tektronix/SITe. These CCDs are used for imaging, spectroscopy and adaptive optics applications. The main goal of developing FIERA was to achieve the best performances possible with present and future developments in CCD technology. Over the last 3 years 11 optical detector systems have been delivered to the telescope with readout speeds up to 625 kilopixel per second per port and a read noise performance under 2 electrons rms at a readout speed of 50 kilopixel per second per port. With automated equipment and routines, we are able to undertake a broad range of tests with minimal manual interaction involved. This paper reviews the current performance and results obtained with the CCDs in the lab and under telescope operations.

1. INTRODUCTION

The Optical Detector Team (ODT) at ESO is committed to provide a large amount of optical detector systems for various instruments to take full advantage of the unique state-of-the-art telescope sites in Chile. Most optical instruments for the Very Large Telescope (VLT) will be equipped with large "new generation" CCD devices that match a standard format of 2000×4000 pixels with a 15 µm pixel size. These devices have 2 readout amplifiers along the short side and three or four-side buttable packages. Up to now, ESO has concentrated on EEV and MIT/LL devices, which match this format. 2K×2K devices from Tektronix and SITe have been implemented on 2 instruments.

For an adaptive optics application ESO signed a contract with EEV to manufacture a custom designed 128×256 pixels, split frame transfer device with 24 µm pixel size and 16 readout ports. Another contract was signed with the University of Hawaii consortium for the MIT/LL CCID-20 and a custom designed CCD for curvature wavefront sensing. This CCD is produced by MIT Lincoln Laboratory.

An overview of the CCD systems delivered by the ODT from 1997 to 1999 is shown in the tables 1 to 3 of James Beletic's paper in these proceedings [6]. In the following sections we present an overview of the performances achieved with those devices at ESO.

2. EEV DEVICES

2.1 EEV CCD44-82

One of the baseline devices used at ESO is the EEV44-82. The geometrical dimension and specifications are:

- Backside, single layer anti reflection coating
- Full frame and frame transfer capable
- 15×15 µm pixel size, 100% photosensitive
- Number of photosensitive pixels: 2048×4102 [H×V]
- Size of the photosensitive area: 30.72×61.53 mm
- 2 output amplifiers
- 50 horizontal prescan pixels in the serial register.
- A dump gate for fast wiping
- A four side buttable package

Each device has non-light sensitive areas at its borders: 100 µm at the top, 450 µm on the left and right sides. At the bottom, a 2.5 mm space is used for the bonding wires. For example for the wide field imaging 8K×8K mosaic, the individual EEV CCDs were put next to each other with a gap of 0.5 mm. This adds up to a non-light sensitive area of 1.4 mm in horizontal direction and 0.7 mm in the vertical direction in the mosaic.

2.1.1 Noise performances

Table 1 lists the noise performance achieved with the EEV44-82 at different readout speeds and conversion factors (e^-/ADU). The noise was measured with the instrument under full operations at the telescope.

Table 1. Noise performance of the EEV44-82 devices at ESO

Speed [kps]	Conversion factor [e^-/ADU]	Readout Time[1] [sec]	Noise [e^- rms]	Instrument
50	0.54	170	1.9	UVES /VIMOS
225	0.54	38	3.2	UVES /VIMOS
325	2.0	27	4	WFI
625	1.64	14	4.7	VLT test Camera 2

[1]Full array, 1 port

The noise figures may vary slightly (~10%) for different devices. Conversion factors less than 1 e^-/ADU are mainly used for spectroscopy applications, whereas higher conversion factors are used for imaging applications.

The ODT employs a special procedure that allows fine-tuning of the VOD, VDR and JD voltages (3D-voltage cube) to get the best compromise between noise and linearity values.

2.1.2 Quantum efficiency (QE)

EEV has optimized the anti-reflection (AR) coating of the EEV44-82 to get good QE in the B and U bands of the spectrum. Nevertheless, the relative QE varies by 5-10% for the different devices. This is due to thickness variations of the backside anti-reflection coating, which is hafnium oxide with a 50 nm mean thickness.

We measured the absolute QE for 12 EEV44-82 devices and derived an average plot as seen in figure 1. For wavelength above 650 nm, the QE is extremely stable. In addition the QE curve for the most sensitive device in the ultraviolet is shown. This CCD was then selected for the blue arm of the UVES instrument. All the QE curves have been obtained with the ESO CCD Testbench [1].

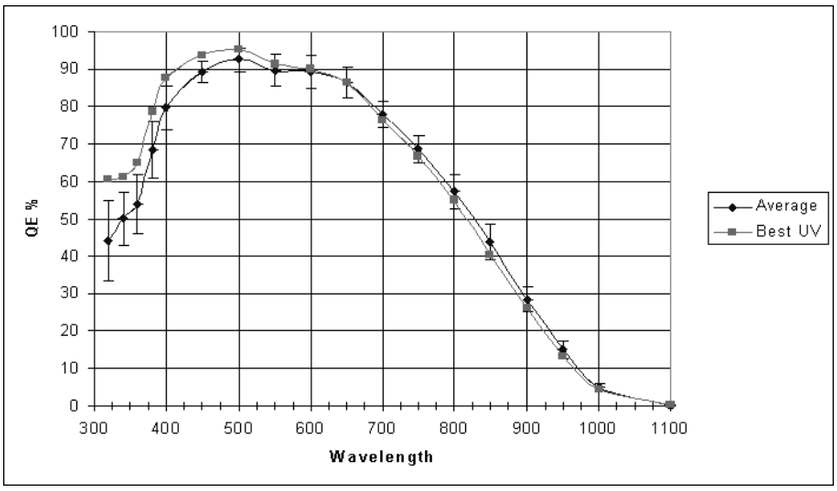

Figure 1. Average QE of 12 EEV44-82 devices. Error bars show the QE standard deviation.

2.1.3 Photo Response Non Uniformity (PRNU)

Fringing patterns in a CCD image make the flat-fielding process of the image difficult, especially for images taken with a spectrograph. The ODT has quantified the fringing effect on 8 EEV44-82 devices by measuring the Photo Response Non Uniformity (PRNU) across the chip. The PRNU in the near infrared (NIR) is related to the thinning of the CCD and the aperture (F/#) of the incoming beam. The more the beam is open, the less the fringing is visible. In the blue part of the spectrum the PRNU degrades due to the backside p+ implementation laser annealing. The images in figure 2 show qualitatively these effects. Figure 3 plots the average PRNU for 8 EEV44-82 CCDs.

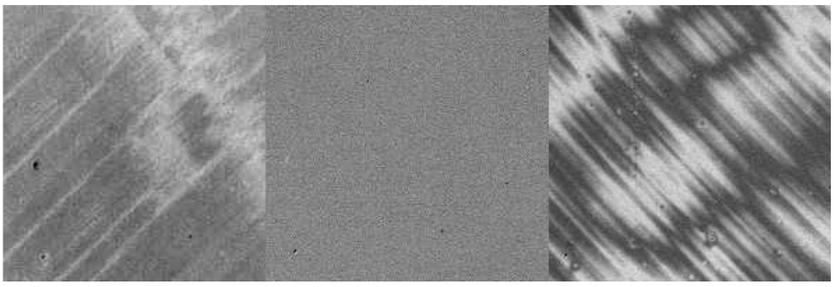

Figure 2. Flat fields of a 300×300 pixels area on the detector (F/2 beam and 5nm bandwidth). The positive images have wavelength settings of 320nm, 650nm and 950 nm (left to right).

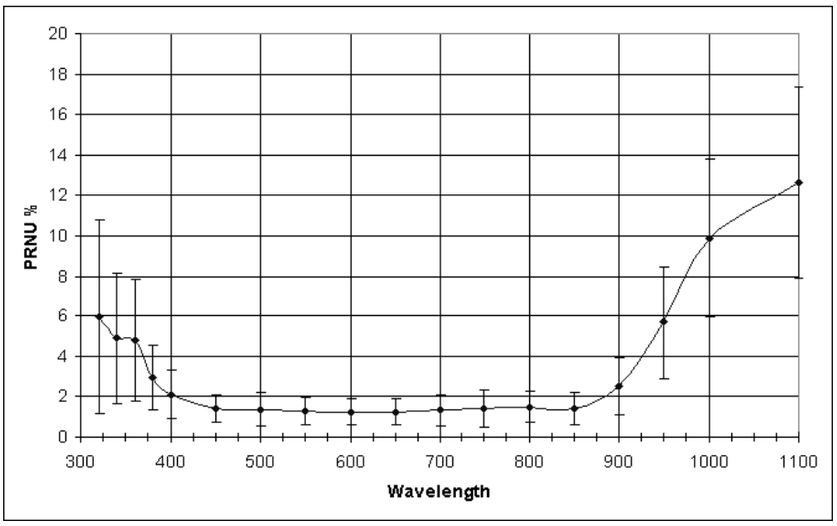

Figure 3. Average PRNU measurement for 8 EEV44-82 CCDs. The error bars show the PRNU standard deviation.

Between 400 nm and 850 nm, the PRNU is very good and almost photon-noise limited. The PRNU was measured on a dust-free area on the chip and taking 10% and 90% of the computed histogram as deviation figures. Below 400 nm, a diamond pattern is visible. This can be flat fielded out easily provided that the CCD temperature is stable within 2-3 degrees. We measured the stability of this diamond pattern with respect to the CCD temperature and for a drift of 20 degrees (170K-150K) we found a 1.25% peak to peak variation for the PRNU. Additional studies on this matter can be found at [2].

2.1.4 Cosmetic defects

The different kinds of defects which degrade the cosmetic quality of the device, can be classified into three categories:

- Defects visible in bias images (mainly hot pixels).
- Defect visible with a low light level flat field (traps).
- Defects visible in the median stack of five 1h exposed dark frames (mainly oversatured hot pixels, trails).

In all cases, a defect is defined as a pixel value above or below 5 sigma from the mean of the neighbouring pixels. These defects are measured to rank the device. A good science grade is typically a device with less than 5 defective columns. The number of defects visible in long dark exposure depends strongly on the CCD operating temperature. From our experience, a temperature of –120°C is best to minimize these effects. Cooling down the EEV CCDs even more does not enhance its cosmetic quality.

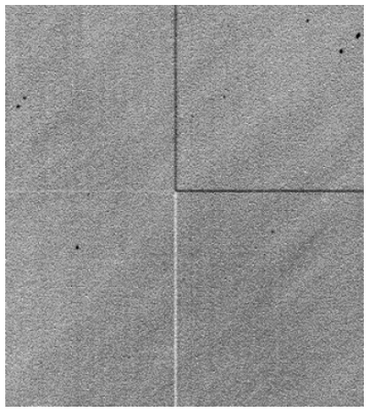

Figure 4. Effect of block stitching between 1K×512 areas

Figure 4 shows an example image of an EEV44-82 which is manufactured using a 1024 by 512 pixels photolithography mask. The area boundaries between those pixel blocks show a 1-2% QE variation over 1 row/column due to the stepper mismatches introduced. These small defects flat field out perfectly and are not temperature dependent.

Finally, the amount of the “defects” induced by cosmic rays should be minimized by the choice of the material used for the CCD package and the head of the detector. The total number of “hits” is typically between 1 and 1.5 event/min/cm^2 for the EEV devices.

2.1.5 Charge transfer efficiency (CTE)

Typically, we measure horizontal CTE of 0.9999995 and vertical CTE of 0.9999988 using the Extended Pixel Edge Response method [1] in the overscan areas. It means that a pixel having 1000 electrons located on the side opposite to the readout port (X=2048, Y=4100) will lose 6 electrons, once the charge packet reaches the readout node (photon shot noise is around 31e$^-$ at this level).

2.1.6 Dark Current

EEV44-82 devices do not have an MPP implant. The dark current is temperature dependent as shown in figure 5. The CCD must be cooled down to a temperature of less than –95°C (180 K) to have dark current less than 5 e-/pixel/hour.

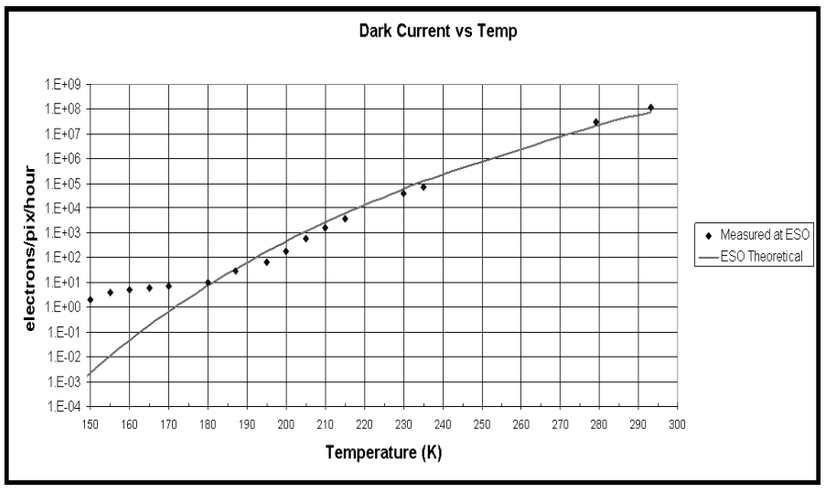

Figure 5. Dark current versus temperature for the EEV44-82 CCDs

Table 2. Dark current measurements

Temperature measured on CCD package [Celsius/K]	Dark current [e^-/pix/hour]
- 102 / 171	20
- 120 / 153	1 or 2

Below 180 K, the measured dark current remains higher than the theoretical value expected, due to a remanence effect, even when the CCD is left in the dark over many hours. This is explained in the next section.

2.1.7 Remanence effect- residual image

A remanence effect occurs when a flat field (mean > 10000 e^-) is taken prior to the dark frame. The resulting effect is an increase of dark current, especially at temperatures lower than 180 K. We are trying to avoid this effect by applying a special wiping sequence (with different parallel voltages). Figure 6 and 7 show a set of 24 one hour dark frames (operating temperature is 160 K). This set was taken after the CCD was fully saturated. It requires four, one-hour dark frames to remove the charge causing the residual image and to reach the nominal dark current value (about 3 to 5 e^-/pix/hour) for this temperature. The remanence effect appears also on dark frames taken after bright star exposures (see figures 8).

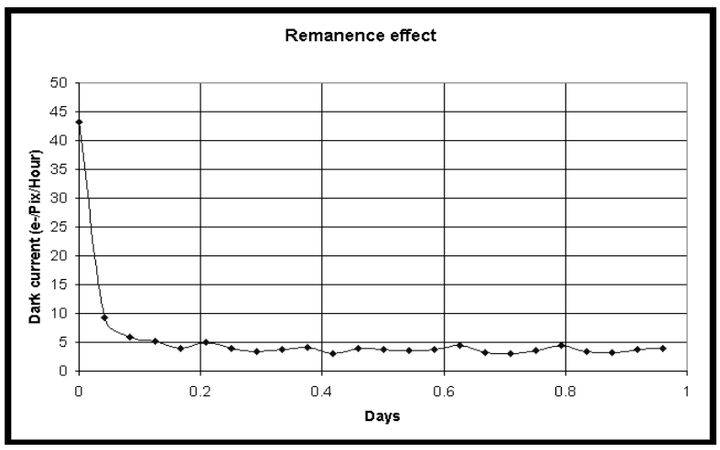

Figure 6. Remanence/residual image effect after flat field taken at t=0

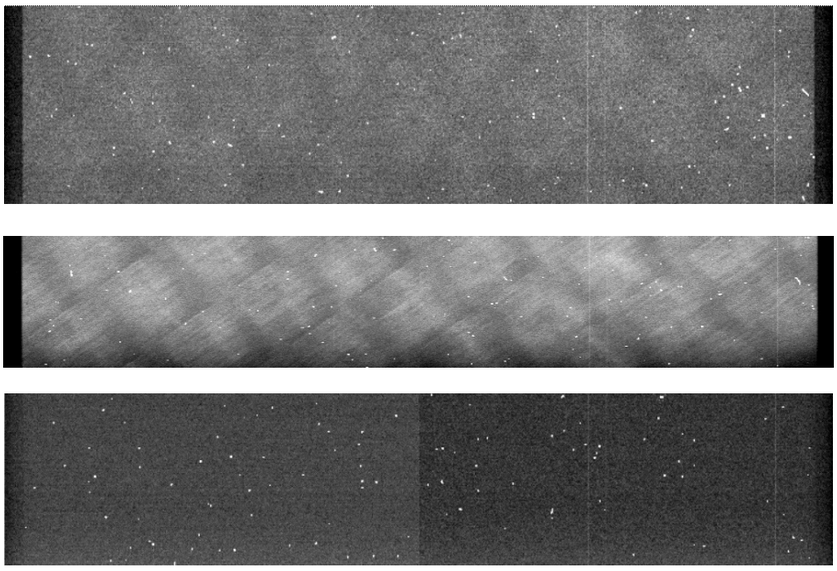

Figure 7. Top: 2048×512 pixel subframe, one hour exposure dark frame, just after a flat field. The dark current is 43e^-/pixel/hour and it is caused by the blue diamond pattern. Center: 2nd 1-hour dark frame, the diamond pattern is fainter, 10e^-/pixel/hour of dark-current. The overscan and prescan areas are visible. Bottom: 28th 1-hour dark frame, dark current has reached the minimum value (4e-/pix/hour) for the operating temperature of 160 K.

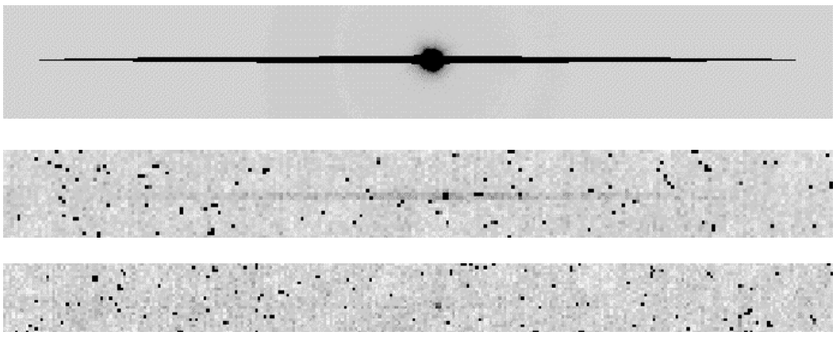

Figure 8. Top: Oversaturated spot and vertical blooming (the serial register is vertical). Center: 1-hour dark exposure, taken immediately after the top frame: binned 10×10, a faint remnant of the star is visible. Bottom: 2nd 1-hour dark exposure: only the central spot is visible.

2.1.8 Amplifier glowing

Our experience shows that voltages less than 25 volts must be applied to the VOD node of the chip to avoid amplifier glowing. The channel voltage is 11V and the substrate voltage is set to 0V.

2.1.9 Linearity

We measured linearity using two different methods. The classical way is to take a set of frames with different exposure times. A new method is the Time Delay Integration (TDI) method. The CCD is read-out while keeping the shutter open. This gives an image with a ramp of intensities ranging from bias level up to saturation. A paper describing this method is in preparation [3]. A good linearity, in the range of 0-100Ke^-, can be achieved without degrading noise performance by optimizing the voltages applied to the CCD readout amplifier. Table 3 and figure 9 summarize typical linearity performances for the EEV devices read out at 225 kilopixel/sec.

Table 3. Linearity of EEV devices, left and right port (225kps), using the "TDI" method

Port	Speed [kps]	Peak-peak [%]	Rms [%]	Range [ADU]	Saturation [Ke^-]
A	225	+0.20 / -0.35	0.15	0-62000	96
B	225	+0.20 / -0.35	0.15	0-62000	95

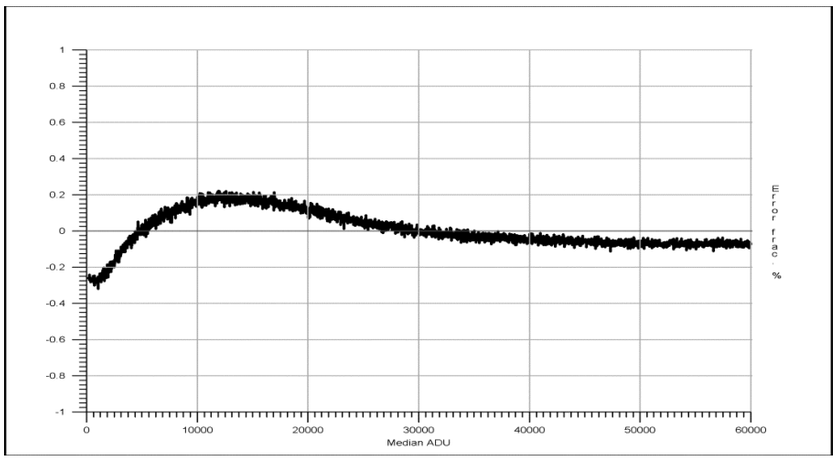

Figure 9. Non Linearity residual plot using the TDI method

A special voltage optimization (named "voltage cube") is used to get at least ±0.5% non-linearity up to full well. The voltage cube is independently tuning three critical voltages of the CCD (output drain, reset drain and JFET drain voltage) in order to minimize the non-linearity with no degradation of the noise performance.

2.1.10 Flatness

A special measurement device was developed to acquire a full chip surface profile [4] for the CCDs. A typical value for the EEV-44 is ± 6 µm at 150 K, a maximum value is ± 10 µm peak-to-peak. Figure 10 shows a typical surface plot.

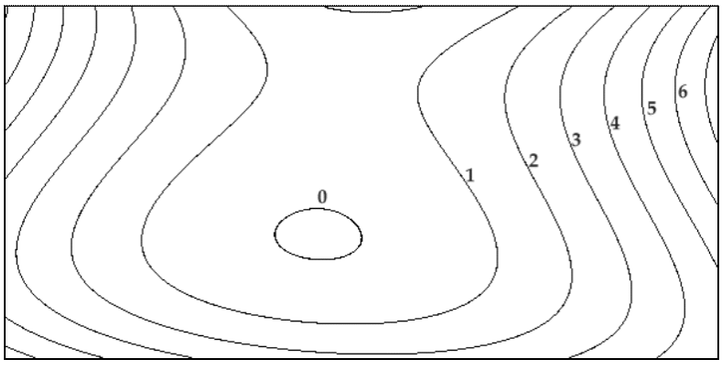

Figure 10. Typical iso-elevation 2 dimensional plot of the CCD surface (units are µm)

2.1.11 Modulation transfer function (MTF)

According to our measurements, the CCDs show no serious degradation from the Nyquist curve. The very sharp hits resulting from cosmic ray impacts show that 95% of the energy released can be measured within one pixel.

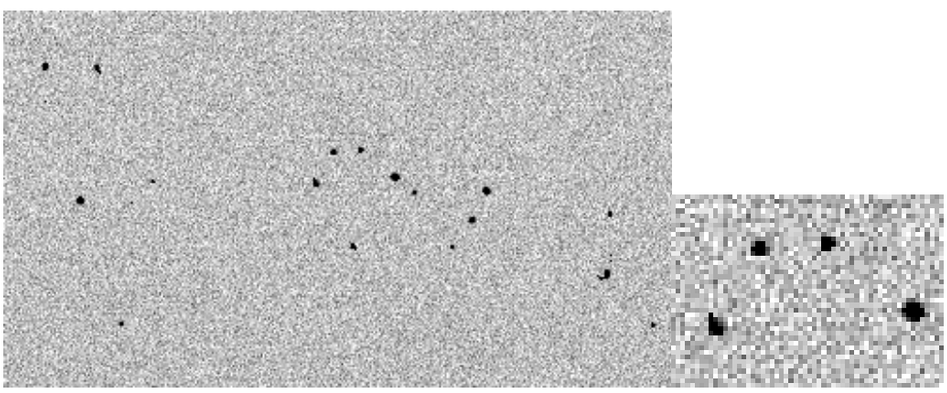

Figure 11. Left: cosmic rays hits (1 hour exposure). Right: enlargement showing 4 cosmic rays hits (Negative images).

2.1.12 Blooming effect

In order to avoid loss of fill-factor, the EEV CCDs do not have an anti-blooming implant. This causes vertical trails over bright and saturated stars. Table 4 gives a rough indication on the number of pixels affected when a point source is oversaturated. L1 denotes the number of pixels affected in the serial register direction, L2 the one in the opposite direction. These measurements were made with binning 1×1 at 350 Kps readout speed.

Table 4. Blooming effect

Direction	**Overexposure factor relative to 150Ke$^-$**							
	2	4	5.8	10	25	50	100	1000
L1(pixels)	0	0	1	2	8	19	39	344
L2(pixels)	0	0	1	3	5	8	13	136

2.2 EEV CCD-50

2.2.1 Architecture and functionality

The optical detector team is in charge of developing a CCD - based visible wavefront sensor for a Shack Hartman - based adaptive optics system (NAOS) [5]. The CCD used is a split frame transfer CCD with a light sensitive area of 128×256 pixels and a pixel size of 24 µm. A storage section, which is 64 rows wide, is located at the top and at the bottom of the sensitive area (figure 12 left). Four additional rows at the base of each storage section compensate for misalignment of the light shield

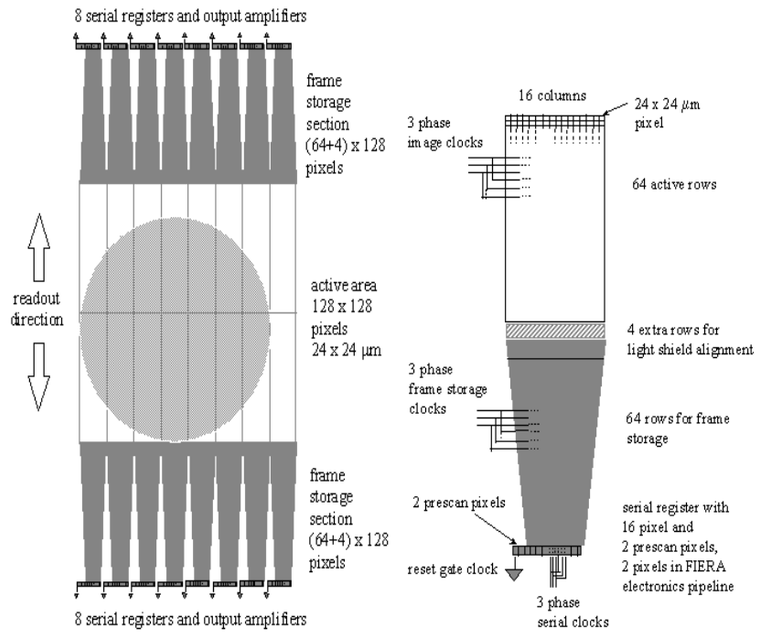

Figure 12. Left: CCD-50 architecture. Right: CCD-50 subsection

The charge is shifted to 8 amplifiers on the bottom and 8 on the topside of the device. Therefore, the CCD is partitioned into 16 sections, each being read out from one amplifier only. Two movable microlens arrays are used to focus the light of the individual subapertures on the CCD. The lenslet arrays, with 7×7 and 14×14 subapertures respectively, are integrated inside the cryostat. A subsection of the CCD with 16×64 pixels of the image zone, the corresponding storage section and serial register are displayed in figure 12 (right).

All these sections are clocked the same way. The clocks are 3 image phases, 3 independent phases for the storage section, 3 clocks for the serial register and a reset gate. Moreover, bias voltages for output gate, the drains of the output amplifier, and the reset MOS-FET have to be supplied. Figure 13 shows an image of the device installed in the CCD head (left) and a dark frame taken with this CCD (right).

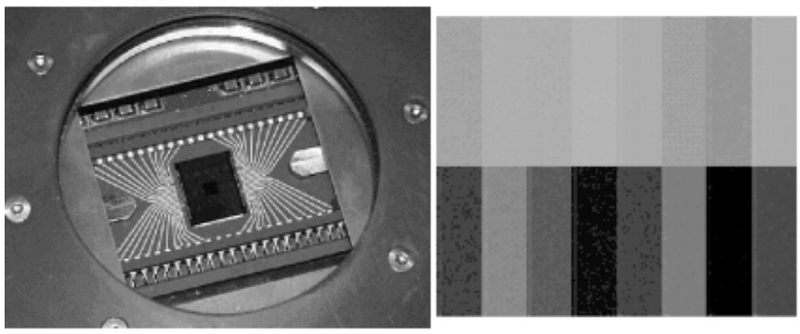

Figure 13. Left: EEV CCD-50, installed in the CCD head. Right: Dark image obtained at 500 frames/second

The CCD-50 is able to operate at up to 1000 frames/sec rate with up to 2 MHz clock speed to 'clear serial register' and 'line shift' operations. For the NAOS application this device is operating in a variety of read modes. 15 to 500 frames/sec are possible with binning options from 1×1 to 4×4 pixels. Moreover, reading selected windows on the subapertures is possible.

The devices tested and implemented so far are virtually defect-free and operated at 180 K. The dark current is negligible at this temperature. The quantum efficiency for the devices is thought to be the same as for the CCD-44 large format CCD but this has been not yet verified. For faint objects, the conversion factor is adjusted to 0.3 electrons/ADU, for brighter objects to 2 electrons/ADU. The readout noise is 3 electrons at 50 kps and 6 electrons at 635 kps.

2.3 MIT CCD performance overview

ESO and MIT/LL are part of the University of Hawaii consortium for the MIT/LL 2K×4K 15µm CCID-20. One of these devices is implemented in the red arm mosaic of the UVES spectrograph [6]. The MIT chip features higher QE in the NIR and reduced fringing compared to the EEV44-82. Figure 14 shows the QE curve for the W7C2 as measured at ESO.

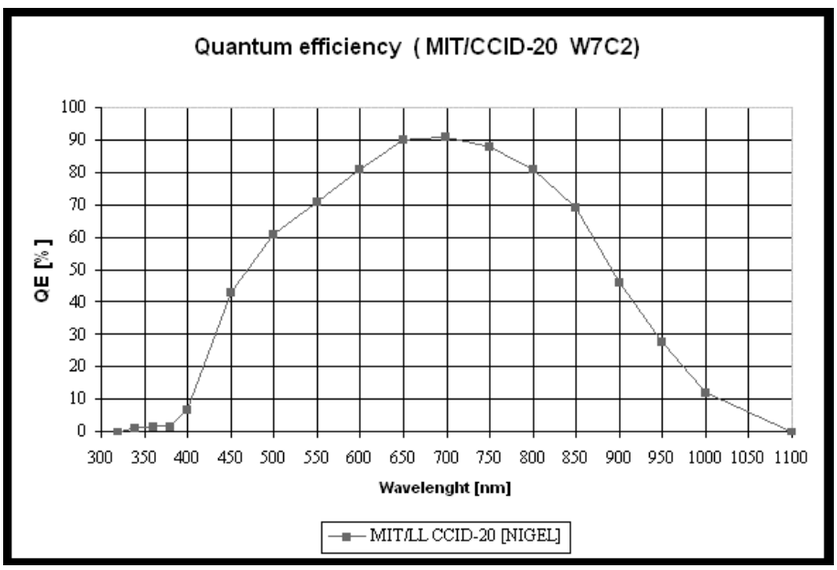

Figure 14. Quantum efficiency of the MIT/LL CCID-20 (W7C2) The QE tops out at over 91% and gives good near infrared QE with over 28 % at 950 nm

2.3.1 Linearity

The device has excellent linearity data up to 625 kps readout speeds. We measured non-linearity residuals of ±0.10 % peak-to-peak at a readout speed of 225 kps (figure 16) and +0.10/-0.08 % peak-to-peak at 50 kps up to a full well of ~100 000 electrons (figure 15).

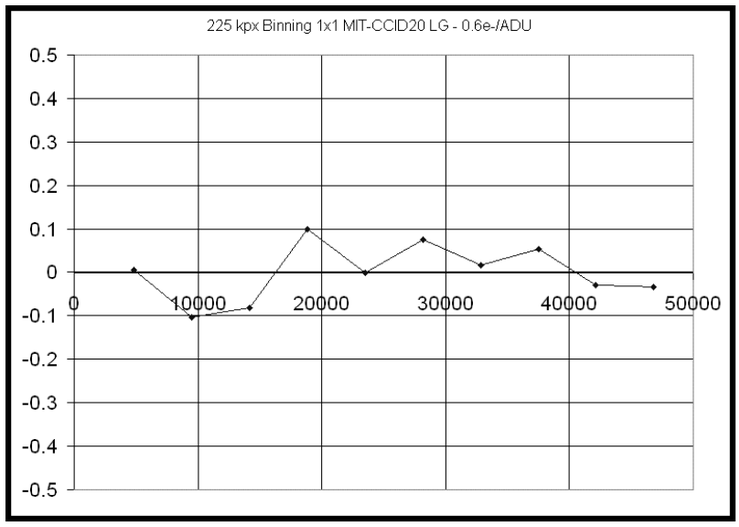

Figure 15. MIT/LL CCID- 20 non linearity residual at a serial register speed of 225 kilopixel per second

2.3.2 Dark current

A dark current of 0.6 e^-/pix/h is measured when the CCD is operated at 155 K at the telescope. This value is reached only after the system is powered on for at least 1 day. Higher values of up to 3 electrons per pixel per hour are measured directly after powering up the system. As explained for the EEV devices in section 2.1.7, this is related to remanence effects.

2.3.3 CTE

Near perfect CTE is achieved using the serial and parallel clocks without generating spurious charge. We measured with both ports better than 0.999999 in both directions.

2.3.4 Cosmetic defects

The device has a good cosmetic quality, with the exception of two partially blocked columns (one of them very short) and one very bright column. The bright column is caused by a single hot pixel in the first imaging column on the left -amplifier side of the CCD. The list of cosmetic defects includes:

- one hot column and 3 traps (low level flat fields).
- 1520 pixels are above 5σ with 2 hot columns (bias frame).
- 2432 pixels are above 5σ, one defect column and very hot pixel + trail and 4 traps are visible (5 1-hour dark frames).
- a “brick wall” pattern is visible at short wavelengths but flat-fields out very easily.

2.3.5 Read out noise

We have only worked with one CCID-20 so far and therefore readout noise has not yet been fully optimized. The latest results from the UVES spectrograph give the following noise performances at different readout speeds for this device:

Table 5. Noise results for the MIT/LL CCID-20

Speed [kps]	Noise [e^-]	Conversion factor [e^-/ADU]
50	2.87	0.57
225	3.69	1.48
625	4.46	1.62

2.3.6 Fringing / Photo-response non-uniformity

The NIR PRNU depends on the fringing effect also for the MIT device. Despite the fact that in this band the MIT CCD, being thicker than the EEV (20 μm instead of 15 μm), should be less affected by it, we measure the same amount of PRNU for both devices.

However, the MIT device has a higher spatial frequency of fringing, which means that the surface of the CCD is flatter and its parallelism is improved (see figure 16, left).

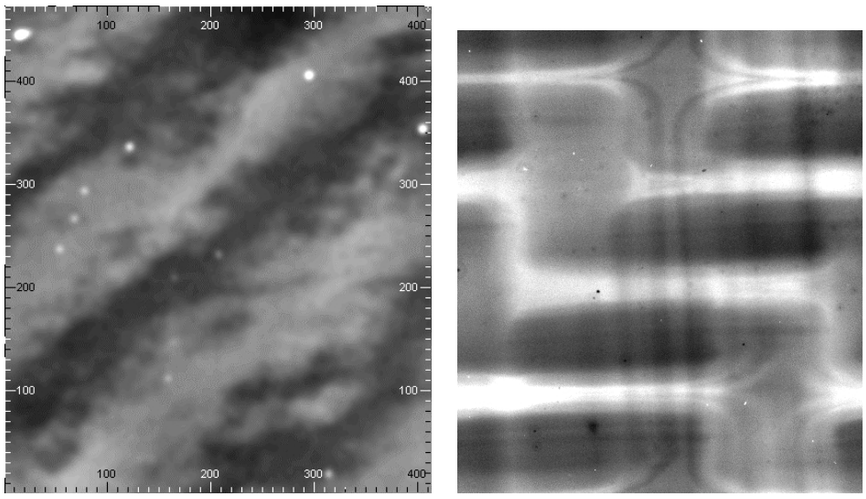

Figure 16. Left: typical image of a NIR (850 nm) fringing pattern (bandwidth=5nm). Right: typical image with a brickwall pattern visible at 350 nm (bandwidth=5nm)

In figure 17, the high PRNU in the wavelength range 300-400nm (up to 40%) for the MIT/LL device is related to the backside laser annealing process (see also the "brick wall" pattern in figure 16 right). The next MIT/LL devices have been manufactured with an enhanced laser annealing process and the brickwall pattern should be reduced.

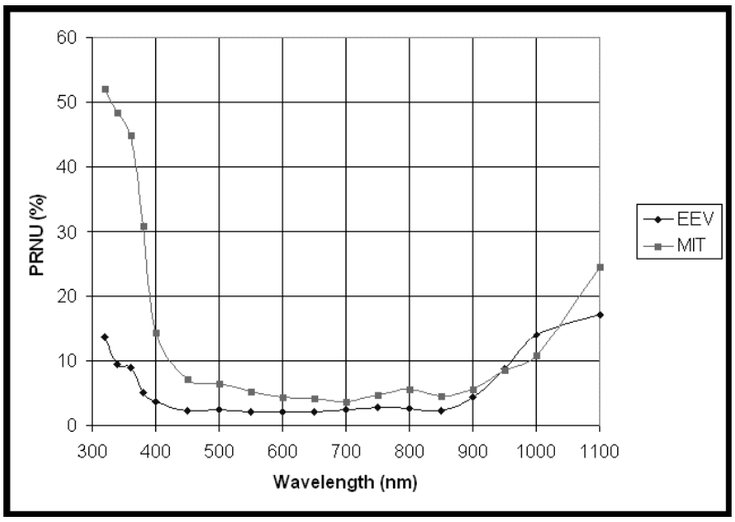

Figure 17. Comparison of PRNU for the CCID-20 and EEV44-82 devices)

2.4 SITe/Tektronix CCD performance overview

A Tektronix 2048 is used for FORS1 (FOcal Reducer and Spectrograph) and a SITe 442A CCD is used for FORS2. Both CCDs are thinned, 24-µm pixel size devices with 4 readout port. Table 6 summarizes the performances achieved with the SITe CCD.

Table 6. SITe CCD performance data in a nutshell

	Unit	Value	Comments
Noise	e^- rms	5.2	@ 50kps, 1.8 e^-/ADU, Port A
Linearity	% peak-to-peak	+0.45/-0.48	@ 50kps, 1.8 e^-/ADU, Port A
Linearity	% rms	0.23	@ 50kps, 1.8 e^-/ADU, Port A
Dark current	e^-/pix/hr	4.2 +/- 0.4	@-110C
CTE	-	0.999999995	Vertical CTE to Port A/B
CTE	-	0.99999981	Horizontal CTE to Port A

At 100 kps we measured 9 e^- and at 200 kps 15 e^- noise. The PRNU of the science device is 7% at 350 nm, 2% at 500 nm and 5% at 950 nm. The blue PRNU is mainly due to AR coating non-uniformity and also a coating defect is visible on the upper left corner.

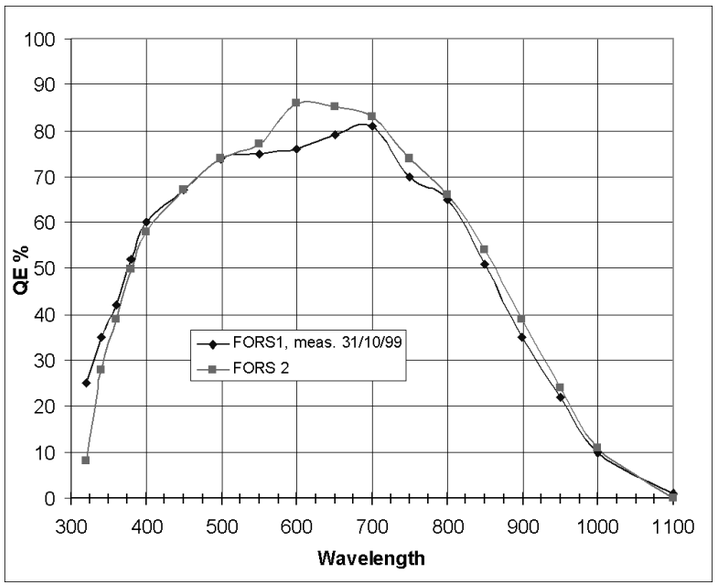

Figure 18. QE of the SITe442A 2K×2K device used in FORS2 and the TK 2048 used in FORS1.

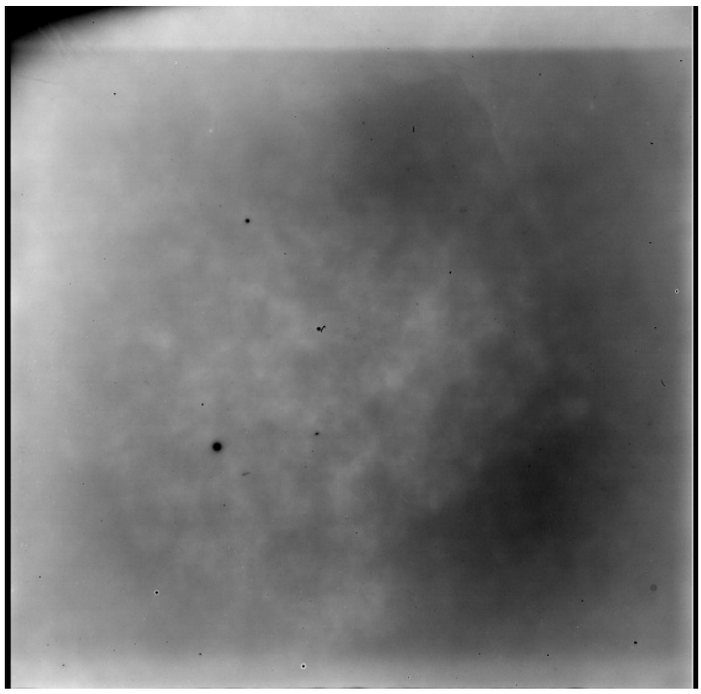

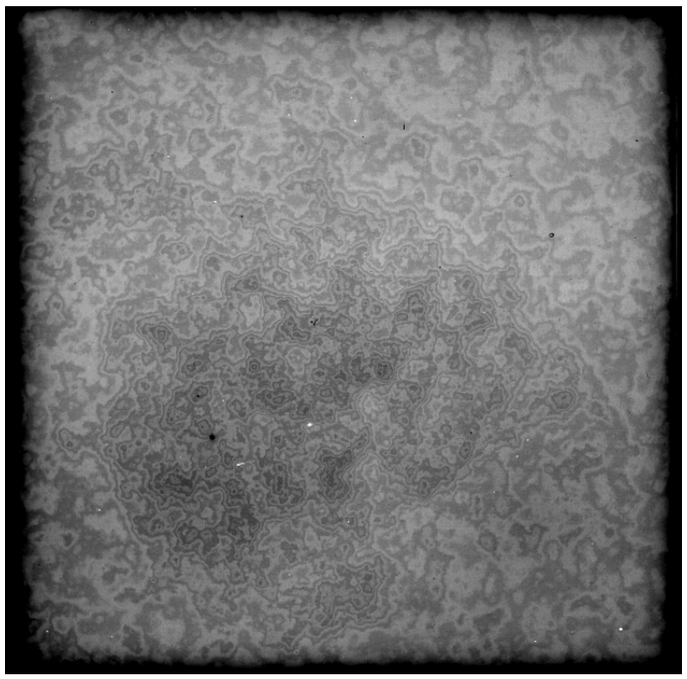

Figure 19. Top: flat field image at 350 nm, 5 nm bandwidth. Bottom: flat field image at 950 nm, 5 nm bandwidth.

3. A NEW CCD FOR CURVATURE WAVEFRONT SENSING

ESO has a new contract via the University of Hawai with MIT/LL to produce a custom designed CCD device (CCID-35) for curvature wavefront sensing [7]. The motivation is that ESO is making six 60-element curvature systems for the VLT and computer simulations showed that a CCD could replace avalanche photo diodes (APDs) as a detector for curvature wavefront sensing [8,9]

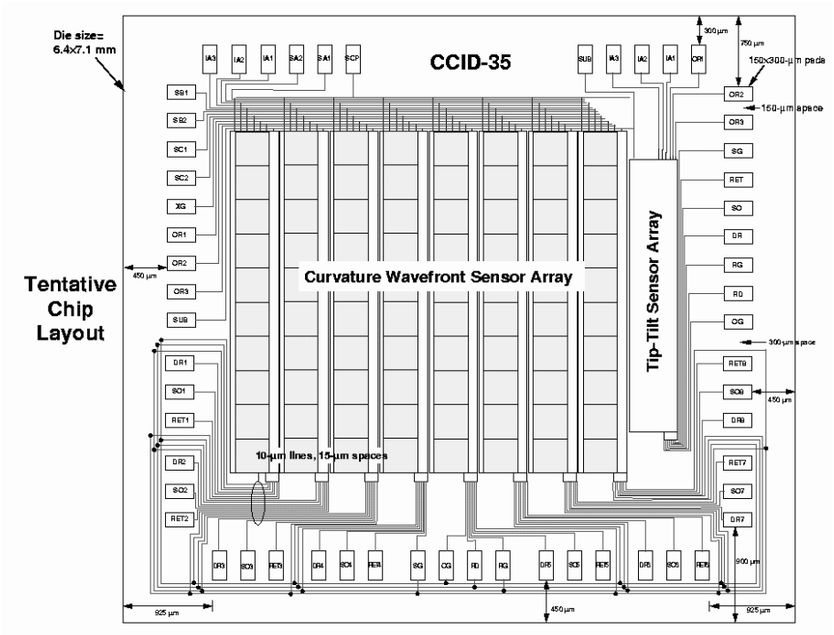

Figure 20. Layout of the CCID-35 designed for curvature wavefront sensing

The device features a unique ability to store charge while reading and integrating with multiple readout ports. The device also features a separate CCD column to allow independent tip tilt sensing. The CCD has a “superpixel” architecture of 80 superpixel. Each superpixel is an imaging section of 20×20 pixels with 18µm pixel size. Each superpixel has 3 storage sections to allow charge to be added on chip over more integration

cycles. Very short exposures (250µs) with "long" integration times (1 to 20 ms) are possible. Figure 20 shows the design for the device. The device has the same amplifier as the CCID-20 followed by a U309 JFET transistor for high responsivity (20 µV/e^-). A readout noise better than 2 electrons and high quantum efficiency with peaks greater than 90% is expected.

4. CONCLUSIONS

A wide range of CCDs have been employed and tested at ESO during the last three years. Concerning CCDs used for spectroscopy and imaging application, we mainly use EEV CCDs. Given the large number of devices delivered to us, we could test their performances in great detail. Those are very high-end performance devices with very good quantum efficiency (optimized for U, B and V band), fast readout, low noise and almost no cosmetic defects. The single MIT device is also extremely promising in terms of noise and speed. The CCDs for adaptive optics are still in the testphase, but show a very high level performance already in the laboratory. Combined with the newly developed FIERA CCD controller, these CCDs contribute to the state of the art instruments installed at ESO's Observatories. The success of these detector systems was only possible due to the excellent work of all people in the Optical Detector Team at ESO.

5. REFERENCES

[1] Paola Amico and Torsten Böhm, ESO's new CCD testbench, *Optical Detectors for astronomy*, James Beletic and Paola Amico eds, Kluwer Academic Publishers, p 95.

[2] Floris Crompvoets-Stephen Smartt, ING Technical Note #123, Wavelength Dependant Pixel to Pixel Response variation of a typical EEV42-80 CCD : The role of flat-fielding astronomical data. (Isaac NewTon Group, La Palma), Paper found in the LaPalma CCD group web page

[3] Cyril Cavadore and B. Gaillard, in preparation.

[4] Stroebele, Stephan "A new machine for planitary measurements of CCDs and mosaics of CCDs", these Proceedings, page XXXX

[5] Feautrier, P. and R. J. Dorn, (2000). "NAOS visible wavefront sensor", *Adaptive Optical System Technology*, SPIE Proceedings vol. 4007.

[6] Dorn R.J., J.W. Beletic, C. Cavadore and J.L. Lizon (2000), "The optical detector systems for the blue and red arms of UVES, the echelle spectrograph for the UT2 Kueyen Telescope at the ESO Paranal Observatory", *SPIE Proceedings* vol. 4008.

[7]. Beletic James W., Reinhold J. Dorn, Thomas Craven-Bartle and Barry Burke, A new CCD designed for curvature wavefront sensing, these Proceedings, page XXXX

[8] Craven-Bartle, T.V. (2000). Modelling curvature wavefront sensors in adaptive optics. Master's thesis, Dept. of Applied Physics, Linköpings Universitet (Sweden).

[9] Craven-Bartle, T.V., Dorn, R.J. and J.W. Beletic, (2000). "Computer simulation of CCDs and APDs for curvature wavefront sensing. In: *Adaptive Optical System Technology*", SPIE Proceedings, vol. 4007.